

Anomalous Hall Crystals in Rhombohedral Multilayer Graphene I: Interaction-Driven Chern Bands and Fractional Quantum Hall States at Zero Magnetic Field

Junkai Dong (董焱轶)^{1,*} Taige Wang,^{2,3,*} Tianle Wang,^{2,3,*} Tomohiro Soejima (副島智大)¹ Michael P. Zaletel,^{2,3} Ashvin Vishwanath,¹ and Daniel E. Parker²

¹*Department of Physics, Harvard University, Cambridge, MA 02138, USA*

²*Department of Physics, University of California, Berkeley, CA 94720, USA*

³*Material Science Division, Lawrence Berkeley National Laboratory, Berkeley, CA 94720, USA*

Recent experiments on rhombohedral pentalayer graphene flakes with a substrate induced moiré potential have identified both Chern insulators and fractional Quantum Hall states in the absence of an applied magnetic field. Surprisingly, these states are observed in strong displacement fields where the effects of the moiré lattice are weak, and seem to be readily accessed without fine-tuning. To address these experimental puzzles we study an interacting model of electrons in this geometry, first within the self-consistent Hartree-Fock (SCHF) approximation. We find an isolated Chern band with Chern number $|C| = 1$, that moreover is relatively flat and shows good quantum geometry. Exact diagonalization and density matrix renormalization group methods at fractional filling establish the presence of fractional quantum anomalous Hall (FQAH) states. The $|C| = 1$ band in SCHF is remarkably robust to varying microscopic parameters, and is also found in the $N_L = 4$ and $N_L = 6$ layer systems. Remarkably, it appears stable even to switching off the moiré potential, pointing to spontaneous breaking of translation symmetry. We term this topological crystalline state the “anomalous Hall crystal” (AHC), and argue that it constitutes a general mechanism for creating stable Chern bands in rhombohedral graphene. Our work elucidates the physics behind the recent rhombohedral pentalayer graphene observations, predicts the appearance of the same phase in other systems, and opens the door to studying the interplay between electronic topology and spontaneous translation symmetry breaking.

Introduction— Tunable experimental platforms that host correlated topological states are fertile grounds for exotic phenomena. In recent years, numerous examples come from moiré heterostructures, where a plethora of platforms have arisen, including twisted graphene multilayers [1–30], twisted transition metal dichalcogenide (TMD) [31–38] bilayers, and rhombohedral multilayer graphene [39–59]. Their menagerie of strongly-correlated phases includes superconductivity [6, 30, 47–49, 60], and fractional Chern insulators (FCIs) [34–37, 42, 46, 61].

Rhombohedral multilayer graphene systems with $N_L = 2 - 5$ layers have presented a diverse array of topological phases, both with [40, 41, 45] and without [39, 43, 44, 55] moiré potentials due to an hBN substrate. Theoretical studies have examined the form of the hBN moiré potential [62–65], and the resulting topological bands [56–59, 66, 67]. In a recent experiment [42], it was reported that rhombohedral pentalayer graphene aligned to an hBN substrate hosts a $|C| = 1$ quantized anomalous Hall (QAH) insulator, and a whole series of fractional quantum anomalous Hall (FQAH) states in the presence of a strong displacement field.

Finding Chern bands that are favorable to realize such fractional states is an ongoing challenge. In initial realizations of fractional Chern insulators, the Chern bands were created by the interplay of a strong magnetic field with a superlattice potential [46]. Later, in the FCIs observed in twisted bilayer graphene [68], a small magnetic

field was only needed to improve the properties of the Chern band [69], which were theoretically predicted to host fractional phases [70–72]. A fractional quantum Hall state at zero field, termed the fractional quantum anomalous Hall state, was only recently realized in MoTe_2 [34–37]. For all of the aforementioned systems, the interaction is necessary to obtain the fractional states, but the presence of Chern bands had been understood at a single-particle level, with interactions establishing spin and valley polarization [73–77]. In contrast, the origin and the character of the Chern band in rhombohedral pentalayer graphene [42] has so far been a mystery.

In this work, we shed light on this mystery by numerically solving the interacting many-body problem. Using self-consistent Hartree-Fock (SCHF) calculations, we find that the interaction-induced gap stabilizes a $C = -1$ state at $\nu = 1$. Using exact diagonalization (ED) and density-matrix renormalization group (DMRG) calculations, we confirm that this Chern band indeed hosts an FQAH state.

The Chern band is remarkably robust to perturbations. Indeed, we find similar Chern bands for different moiré potentials, different hopping parameters for rhombohedral graphene, and even for $N_L = 4$ and $N_L = 6$ rhombohedral layers (Fig. 1(c)). In fact, we find that the state persists even as moiré potential is turned off, within the SCHF approximation (Fig. 1(b), 3(a)(d)). This is reminiscent of the “Hall crystal” phase proposed in [78, 79], where electrons in a magnetic field crystallize into a state that has nonzero Hall conductance. Thus, we propose that the Chern insulator at $\nu = 1$ should be understood as an anomalous Hall crystal (AHC) state that spon-

* These authors contributed equally.

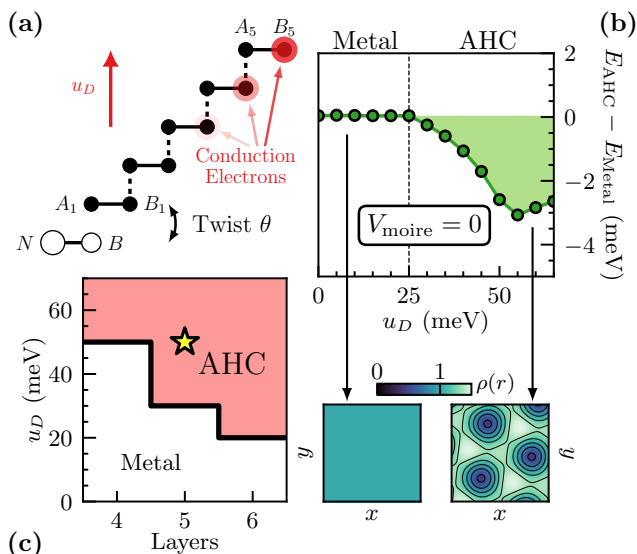


FIG. 1. (a) Geometry of rhombohedral pentalayer graphene on hBN. The bottom layer of rhombohedral pentalayer graphene sits on top of hBN with a relative twist θ . Positive potential differences $u_D > 0$ between layers polarizes conduction electrons away from the hBN layer. (b) The energy difference per electron between translation symmetric metal and anomalous Hall crystal (AHC) within SCHF as a function of u_D in rhombohedral pentalayer graphene with zero moiré potential $V_1 = 0$. The AHC becomes the ground state of the system beyond $u_D > 25$ meV. We also show the typical charge density distribution of the metal and the AHC phases, where the latter exhibits spontaneous translation symmetry breaking. (c) Phase diagram of rhombohedral multilayer graphene for $N_L = 4 - 6$ layers with phase boundary from SCHF. The critical displacement field u_D^* decreases with increasing N_L . The location of the experimentally relevant point is marked by a star.

taneously breaks both continuous translation symmetry and time reversal symmetry (Fig. 1(c)). This establishes an entirely new mechanism for Chern band formation that arises from the interplay of translation breaking and topology.

This interpretation of the state as an AHC clarifies the experimental mystery. Experimental phase diagrams in [42] are strongly asymmetric between positive and negative displacement fields D . This suggests that the hBN is only aligned on one side (Fig. 1(a)). Comparing experimental data at $\nu = 4$ [42] to SCHF calculations of the charge gap (App. B 3), we infer that the Chern insulator appears when the electrons are polarized away from the hBN potential (moiré distant) instead of toward the hBN potential (moiré proximate). We thus expect the hBN moiré potential to have a weak effect on the many-body ground state in the regime where the Chern physics and FQAH effect is observed. This is consistent with spontaneous translation symmetry breaking, where the moiré potential simply serves as a pinning field.

Microscopic Model— We consider a model of N_L -layer

rhombohedral graphene [80, 81] with a moiré potential [62] to account for the hBN substrate at relative angle θ (Fig. 1(a)). The superlattice scale and orientation is set by the graphene-hBN lattice mismatch and θ . The Hamiltonian is

$$\hat{H} = \hat{h}_{\text{kin}} + \frac{1}{2A} \sum_{\mathbf{q}} U_{|\mathbf{q}|} : \hat{\rho}_{\mathbf{q}} \hat{\rho}_{-\mathbf{q}} :, U_{\mathbf{q}} = \frac{2\pi \tanh(qd)}{\epsilon_r \epsilon_0 q} \quad (1)$$

where $\hat{\rho}_{\mathbf{q}}$ is the density operator, A is the sample area, and the normal ordering is relative to the gap of rhombohedral graphene at charge neutrality in the presence of displacement field, $U_{|\mathbf{q}|}$ is the double gated Coulomb potential with a gate distance $d = 250$ Å and ‘bare’ dielectric constant $\epsilon_r = 5$ (unless otherwise specified).

The kinetic term in the K -valley takes the form

$$h_{\text{kin}} = h_{RG}^{(N_L)} + h_D + V_{\text{hBN}}, \quad (2)$$

where $h_{RG}^{(N_L)}$ is a standard model [41] for N_L -layer rhombohedral graphene parametrized by in-layer and interlayer hopping parameters $(t_0, t_1, t_2, t_3, t_4) = (3100, 380, -21, 290, 141)$ meV. The displacement field creates a potential difference of u_D per layer with the zero point at the middle, resulting in layer-dependent potential $[h_D]_{\ell\ell'} = u_D(\ell - 1 - (N_L - 1)/2)\delta_{\ell\ell'}\sigma^0$. Physically, $u_D > 0$ polarizes electrons in the conduction band away from the hBN moiré potential. The moiré potential acts only on the bottom layer with the form

$$V_{\text{hBN}}(\mathbf{r}) = V_0 \sigma^0 + V_1 \mathbf{f}(\mathbf{r}, \psi) \cdot \boldsymbol{\sigma} \quad (3)$$

where V_0 shifts the electronic potential of the layer, V_1 controls the strength of moiré periodic potential, and $\sigma^{0,x,y,z}$ are sublattice Pauli matrices. The function $\mathbf{f}(\mathbf{r}, \psi)$ is a sum of first harmonics, containing a scalar potential, effective mass, and pseudo-vector potential, where the angle ψ controls the phase of the first harmonics [62]. While a variety of models have been proposed for the hBN model [62–65], we find that the physics of the moiré distant side discussed in this work is largely model-independent. As the displacement field and moiré potential break the C_{2x} and M_x symmetries of standalone rhombohedral graphene, the moiré Hamiltonian \hat{H} has only C_{3z} rotation, time-reversal, and moiré translation symmetries. See App. A for full details of the model.

Interaction-Induced Chern Band— To understand the origin of the Chern insulator, we performed self-consistent Hartree-Fock (SCHF) calculations on up to 48×48 moiré unit cells. We project the $N_L = 5$ graphene layers to the lowest 7 conduction bands, which is well-controlled whenever $|u_D|$ is sizable. The relevant Chern insulator recently observed in rhombohedral pentalayer graphene was at electron filling $\nu = 1$ and deep inside the spin valley polarized regime [42]. Therefore we assume polarization to a single valley and spin flavor.

We first consider $u_D = 50$ meV, which we estimate to correspond to $D/\epsilon_0 = 0.81$ V/nm used to stabilize the

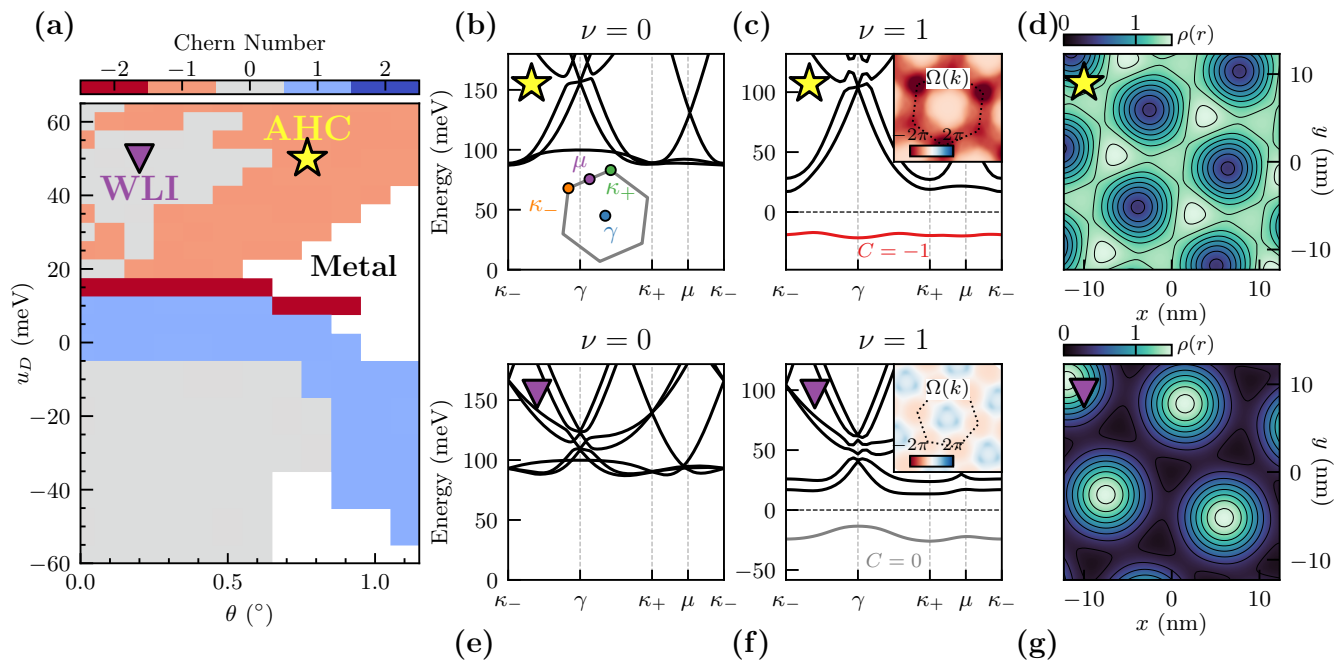


FIG. 2. (a) The phase diagram of moiré rhombohedral pentalayer graphene as a function of the interlayer potential difference u_D , and the twist angle θ . The colors label the Chern number of the SCHF ground states, with gapless regions shown in white. On the moiré distant side ($u_D > 0$), the anomalous Hall crystal (AHC) phase has $C = -1$, whereas the Wigner-like insulator (WLI) has $C = 0$. (b,e) Non-interacting band structures at the yellow star ($u_D = 50$ meV, $\theta = 0.77^\circ$) and purple triangle ($u_D = 50$ meV, $\theta = 0.2^\circ$). Inset in (b): plot of the moiré Brillouin zone. (c,f) SCHF bandstructure at $\nu = 1$, finding an AHC and WLI at the yellow star and purple triangle respectively. Insets: Berry curvature $\Omega(\mathbf{k})$ of the occupied band. (d,g) Charge densities $\rho(\mathbf{r})$ of the AHC (d) and WLI (g). The AHC charge density resembles a honeycomb lattice, whereas the WLI charge density resembles a triangular lattice.

$|C| = 1$ insulator in experiment [82]. At this $u_D > 0$, the moiré distant electrons predominantly occupy the layer away from the moiré potential (Fig 1(a)). Fig. 2(b) shows the single particle bandstructure, which *does not* have a direct gap above the first band. Within SCHF at $\nu = 1$, Fig. 2(c), a direct gap opens of order the interaction scale, whose occupied band (red) has Chern number $|C| = 1$. Its narrow 6 meV bandwidth and favorable quantum geometry, discussed below, make it eminently suitable for fractional topological phases.

Phase Diagram at $\nu = 1$ — Fig. 2(a) shows the phase diagram for $N_L = 5$ at filling $\nu = 1$. On the moiré distant side, $u_D > 0$, the AHC phase is stabilized over a broad range of twist angles and displacement fields near the experimentally-relevant point (yellow star). Decreasing the displacement field drives a transition into a metallic phase, consistent with experimental observation [42]. Reducing the twist angle θ instead drives a transition to a $C = 0$ insulator. We refer to this as a “Wigner-like insulator” (WLI), based on its charge distribution $\rho(r)$. Fig. 2(g) shows that $\rho(r)$ varies strongly in the WLI, with peaks on a triangular lattice, reminiscent of the Wigner crystal. The single-particle band structure, Fig. 2(e), reveals why the WLI phase is competitive: at the γ point, the backfolded bands decrease in energy as θ decreases, bringing many within 30 meV of the minimum. These

bands may then be strongly mixed by interactions, selecting the configuration that minimizes Hartree energy, i.e. a triangular lattice. On the other hand, the AHC state has a weak variation in charge density Fig. 2(d), and has a triangular lattice of minima instead of maxima. The single particle band structure shows a large direct gap at the γ point, consistent with weak translation symmetry breaking of the AHC state.

On the moiré proximate side $u_D < 0$, Fig. 2(a) shows the dominant phase is a $C = 0$ insulator. Though this is consistent with experiment [42], we caution that precise form of the moiré potential will determine the phase diagram in this regime; more accurate modelling incorporating lattice relaxation [65] and other *ab initio* modelling [64, 83] may be required. Furthermore, we note that near $u_D \approx 0$, our approximation of projecting to the conduction bands breaks down.

Robustness of Moiré Distant Phases.— We now show that the physics on the moiré distant side is robust to change in microscopic parameters.

We first consider the effect of changing the phase ψ of the moiré potential (Eq. (3)) generated by hBN. Since the system lacks C_2 symmetry, ψ is not pinned to any particular value, and varies between hBN models. We show the phase diagram of the moiré distant side and the moiré proximate side in Fig. 3(a,b). The charge gap and

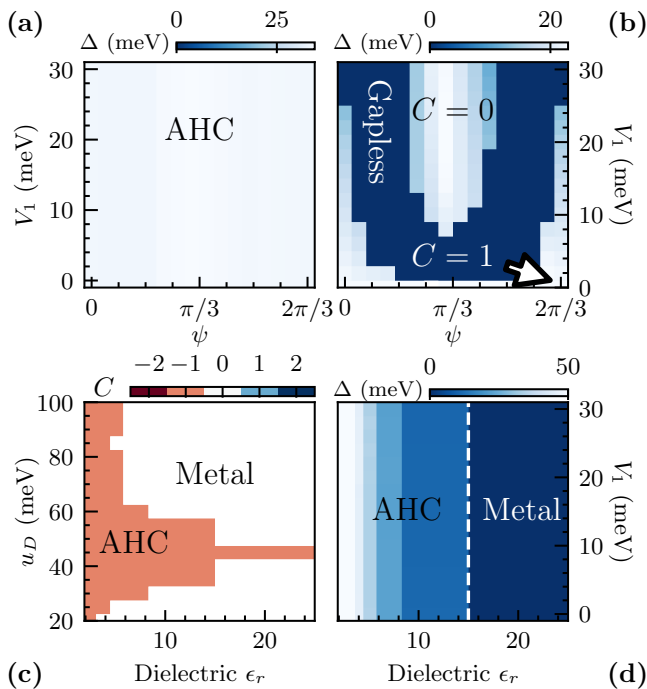


FIG. 3. (a) The featureless charge gap of rhombohedral pentalayer graphene at $\nu = 1$ on the moiré-distant side ($u_D = 50$ meV) as a function of ψ and V_1 . The Chern number $C = -1$ is constant. (b) The charge gap of the moiré-proximate side ($u_D = -50$ meV) as a function of ψ and V_1 . The charge gap closes on a curve in the phase diagram, and the Chern number of the ground state changes based on the strength V_1 and phase ψ of the moiré potential. (c) The Chern number with respect to u_D and dielectric constant ϵ_r on the moiré-distant side, showing the AHC survives to relatively weak interaction strengths near $u_D \sim 50$ meV. (d) The charge gap with respect to the moiré potential V_1 and ϵ_r on the moiré-distant side. The AHC phase extends down to the absence of moiré potential, demonstrating interaction-driven spontaneous translation symmetry breaking. All data at $\theta = 0.77^\circ$.

Chern number of the moiré distant side do not depend on the value of ψ and V_1 , showing that AHC is agnostic to microscopic details of the moiré potential. On the other hand, the charge gap and Chern number of the moiré proximate side changes based on the value of ψ , showing that our uncertainty in the microscopic model strongly impacts the phase diagram in that regime.

The AHC state is further stable to changes in the interaction strength. In Fig. 3 (c) (d), we show the Chern number as a function of u_D and dielectric constant ϵ_r and moiré potential V_1 . The AHC state survives up to $\epsilon_r \sim 15$ for a range of u_D , showing that relatively weak interactions are sufficient to stabilize the state. Moreover, the phase diagram is robust to modelling differences in the hopping parameters of rhombohedral graphene. The AHC phase remains robust even if we turn off all further neighbor hoppings $t_{i \geq 2}$ in the model.

Remarkably, we see the phase survives to a change in

the number of layers of graphene. In Fig. 1(b), we show the extent of the AHC phase at $\nu = 1$ in SCHF for $N_L = 4 - 6$ rhombohedral graphene as a function of u_D . We see $C = -1$ at large u_D for all number of layers. As the number of layers increases, the critical u_D^* decreases significantly, easing the experimental requirement of a large displacement field $D \propto u_D$.

Spontaneous translation symmetry breaking— The resilience of the $C = -1$ phase to the change in moiré potential raises a natural question: Is the moiré potential necessary at all for stabilizing the state? In the following section, we show within SCHF that the ground state is in fact an anomalous Hall crystal [78, 79] that spontaneously breaks translation symmetry.

The electronic structure on the moiré distant side is essentially independent of the moiré potential. Fig. 3 (a)(d) shows that the charge gap hardly changes as a function of V_1 , suggesting the single-particle gap is almost completely due to electronic interactions. This prompts us to consider the Hamiltonian with *zero* moiré potential. Under this condition, the Hartree-Fock calculation finds a ground state with *spontaneously* broken translation symmetry, which has much lower energy than translation symmetric states when $u_D > 25$ meV (Fig. 1(b)). We note that the AHC state is most stable compared to the metallic phase around $u_D = 55$ meV, which is consistent with our estimate for the experimental displacement field. Therefore, the symmetry breaking pattern is completely determined by interaction.

The AHC state is a compressible state in the clean limit, since the lattice constant can change continuously. However, a small spatially-varying potential or disorder can pin its periodicity [79], whereupon its nontrivial Chern number can be revealed through the Streda formula and Hall conductance. This is likely the role played by moiré potential in experiment [42].

Fractional quantum anomalous Hall (FQAH) effect.— One of the main features of the experimental discovery [42] was that a full series of FQAH states were found at fractional fillings in the absence of magnetic field. Employing exact diagonalization (ED) and density matrix renormalization group (DMRG) calculations, here we numerically confirm that partially filling the Chern band generated by the AHC gives us FQAH states.

Recent progress on the study of FQAH phases has emphasized the role of quantum geometry [70, 88–100], in addition to flat dispersion [84–86, 101–103]. Small trace condition violation $T = \int d^2\mathbf{k} (\text{Tr}(g_{FS}(\mathbf{k})) - \Omega(\mathbf{k}))$ gives a band suitable for finding FCIs. Here, $g_{FS}(\mathbf{k})$ is the Fubini-Study metric, and $\Omega(\mathbf{k})$ is the Berry curvature. The AHC band has a combination of flat bandwidth and relatively small trace condition violation (Fig. 4(a)), making it likely to host FQAH phases. Indeed we find that the 1/3 Laughlin state of holes appears at $\nu = 2/3$ of the AHC band, with clear signatures from both ED (Fig 4(b)) and DMRG calculations (Fig 4(d)). We note that these calculations (details in SM) are done in the many-body Hilbert space of the lowest SCHF band at

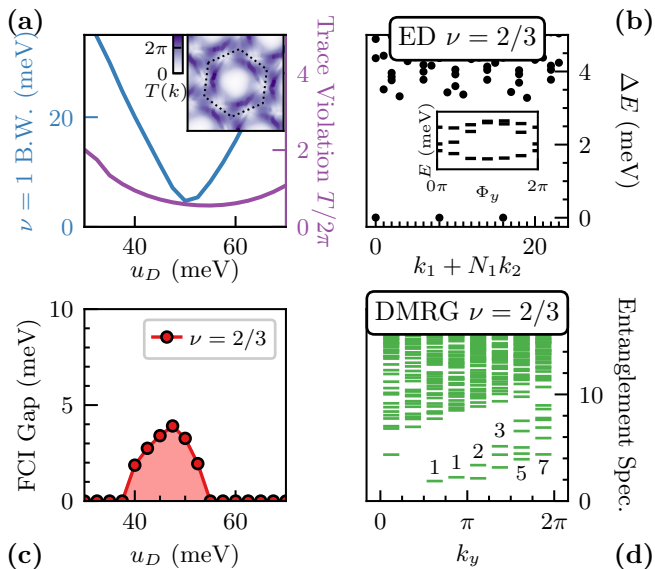


FIG. 4. (a) Band conditions of the AHC phase as a function of u_D . Both the bandwidth and the violation of trace condition are minimized near $u_D = 50$ meV. (b) Many-body spectrum from ED on a 4×6 system at $\nu = 2/3$. Inset: spectral flow of the three degenerate ground states, a signature of the FCI ground state [84–86]. (c) The FCI gap at $\nu = 2/3$ as a function of u_D obtained in ED. The FCI gap is nonzero around 40 to 55 meV, and gives way to metals beyond this regime due to large bandwidths. (d) Entanglement spectrum obtained in DMRG at $\nu = 2/3$ with $L_y = 8$. The partition number counting of states below the entanglement gap is consistent with the chiral edge mode associated with the Laughlin states, confirming the state is an FCI [87]. Parameters: $\theta = 0.77^\circ$, $u_D = 50$ meV unless specified.

$\nu = 1$, assuming spin and valley polarization. The FQAH phase yields to a competing metallic phase small and large u_D (Fig 4(c)).

Examining the stability of the FQAH phases down to the zero moiré potential limit is an excellent topic for future studies, where we expect a competition between an FQAH phase with the same unit cell size, versus Wigner or anomalous Hall crystals with larger unit cells. Experimentally, the existence of the $\nu = 2/3$ plateau points to the realization of the former scenario, at least in the weak moiré potential limit, while a profusion of insulating states at smaller densities might be due to the latter scenario.

Discussion— We have demonstrated the existence of the AHC phase within SCHF calculations. While such a phase can be stabilized *in principle*, SCHF is known to overestimate the tendency to crystallize, for example in Wigner crystals [104]. Pinpointing the location of the phase boundary between the AHC and the metal

with more sophisticated techniques is left to future work. We note that the AHC phase at the optimal u_D survives even after decreasing the interaction strength by a factor of three (Fig. 3 (c,d)), hinting at the robustness of the phase beyond mean-field theory. Previously, an AHC state has been invoked to account for experimental observations on Bernal bilayer graphene [39]. The putative AHC phase there is adjacent to a Wigner crystalline phase, similar to the phase diagram we obtained for rhombohedral pentalayer graphene. While the parameters of the experiment [39] fall outside of what we considered in this paper, it shares similarities to the scenario we examined. This raises the question of whether an FQAH state can be realized in Bernal bilayer graphene by tuning it to an appropriate parameter regime.

The ubiquity of the AHC phase in our phase diagram hints at a universal physical mechanism stabilizing the formation of a Chern band, while the relatively uniform charge density of the AHC state points to a translation-breaking mechanism different from that of the Wigner crystal. A deeper analytic understanding of the origin of the AHC phase is clearly needed, which will be addressed in a forthcoming work.

Note added— Towards the completion of the project, two interesting related papers [105, 106] were posted, which agree with our finding in the areas of overlap.

ACKNOWLEDGMENTS

We acknowledge Long Ju, Tonghang Han, Jixiang Yang, Patrick J. Ledwith, Trithep Devakul, and Bertrand I. Halperin for fruitful and insightful discussions. T.W., T.W., and M.Z. are supported by the U.S. Department of Energy, Office of Science, Office of Basic Energy Sciences, Materials Sciences and Engineering Division under Contract No. DE-AC02-05-CH11231 (Theory of Materials program KC2301). A.V. is supported by the Simons Collaboration on UltraQuantum Matter, which is a grant from the Simons Foundation (651440, A.V.) and by the Center for Advancement of Topological Semimetals, an Energy Frontier Research Center funded by the US Department of Energy Office of Science, Office of Basic Energy Sciences, through the Ames Laboratory under contract No. DEAC02-07CH11358. This research used the Lawrence computational cluster provided by the Lawrence Berkeley National Laboratory (Supported by the U.S. Department of Energy, Office of Basic Energy Sciences under Contract No. DE-AC02-05-CH11231). This research is funded in part by the Gordon and Betty Moore Foundation’s EPiQS Initiative, Grant GBMF8683 to T.S. D.E.P. is supported by the Simons Collaboration on UltraQuantum Matter, which is a grant from the Simons Foundation.

[1] Yonglong Xie, Andrew T. Pierce, Jeong Min Park, Daniel E. Parker, Eslam Khalaf, Patrick Ledwith, Yuan

Cao, Seung Hwan Lee, Shaowen Chen, Patrick R. For-

- rester, Kenji Watanabe, Takashi Taniguchi, Ashvin Vishwanath, Pablo Jarillo-Herrero, and Amir Yacoby. Fractional chern insulators in magic-angle twisted bilayer graphene. *Nature*, 600(7889):439–443, dec 2021.
- [2] Yuan Cao, Valla Fatemi, Ahmet Demir, Shiang Fang, Spencer L. Tomarken, Jason Y. Luo, Javier D. Sanchez-Yamagishi, Kenji Watanabe, Takashi Taniguchi, Efthimios Kaxiras, Ray C. Ashoori, and Pablo Jarillo-Herrero. Correlated insulator behaviour at half-filling in magic-angle graphene superlattices. *Nature*, 556(7699):80–84, mar 2018.
- [3] Petr Stepanov, Ipsita Das, Xiaobo Lu, Ali Fahimniya, Kenji Watanabe, Takashi Taniguchi, Frank H. L. Koppen, Johannes Lischner, Leonid Levitov, and Dmitri K. Efetov. Untying the insulating and superconducting orders in magic-angle graphene. *Nature*, 583(7816):375–378, July 2020.
- [4] Alexandre Jaoui, Ipsita Das, Giorgio Di Battista, Jaime Díez-Mérida, Xiaobo Lu, Kenji Watanabe, Takashi Taniguchi, Hiroaki Ishizuka, Leonid Levitov, and Dmitri K. Efetov. Quantum critical behaviour in magic-angle twisted bilayer graphene. *Nature Physics*, April 2022.
- [5] Petr Stepanov, Ming Xie, Takashi Taniguchi, Kenji Watanabe, Xiaobo Lu, Allan H. MacDonald, B. Andrei Bernevig, and Dmitri K. Efetov. Competing zero-field chern insulators in superconducting twisted bilayer graphene. *Physical Review Letters*, 127(19):197701, November 2021.
- [6] Yuan Cao, Valla Fatemi, Shiang Fang, Kenji Watanabe, Takashi Taniguchi, Efthimios Kaxiras, and Pablo Jarillo-Herrero. Unconventional superconductivity in magic-angle graphene superlattices. *Nature*, 556(7699):43–50, mar 2018.
- [7] U. Zondiner, A. Rozen, D. Rodan-Legrain, Y. Cao, R. Queiroz, T. Taniguchi, K. Watanabe, Y. Oreg, F. von Oppen, Ady Stern, E. Berg, P. Jarillo-Herrero, and S. Ilani. Cascade of phase transitions and Dirac revivals in magic-angle graphene. *Nature*, 582(7811):203–208, June 2020.
- [8] Jeong Min Park, Yuan Cao, Kenji Watanabe, Takashi Taniguchi, and Pablo Jarillo-Herrero. Flavour Hund’s coupling, Chern gaps and charge diffusivity in moiré graphene. *Nature*, 592(7852):43–48, April 2021.
- [9] Yuan Cao, Daniel Rodan-Legrain, Jeong Min Park, Noah F. Q. Yuan, Kenji Watanabe, Takashi Taniguchi, Rafael M. Fernandes, Liang Fu, and Pablo Jarillo-Herrero. Nematicity and competing orders in superconducting magic-angle graphene. *Science*, 372(6539):264–271, 2021.
- [10] Matthew Yankowitz, Shaowen Chen, Hryhorii Polshyn, Yuxuan Zhang, K. Watanabe, T. Taniguchi, David Graf, Andrea F. Young, and Cory R. Dean. Tuning superconductivity in twisted bilayer graphene. *Science*, 363(6431):1059–1064, 2019.
- [11] Yu Saito, Jingyuan Ge, Kenji Watanabe, Takashi Taniguchi, and Andrea F. Young. Independent superconductors and correlated insulators in twisted bilayer graphene. *Nature Physics*, 16(9):926–930, September 2020.
- [12] Dillon Wong, Kevin P. Nuckolls, Myungchul Oh, Biao Lian, Yonglong Xie, Sangjun Jeon, Kenji Watanabe, Takashi Taniguchi, B. Andrei Bernevig, and Ali Yazdani. Cascade of electronic transitions in magic-angle twisted bilayer graphene. *Nature*, 582(7811):198–202, June 2020.
- [13] Myungchul Oh, Kevin P. Nuckolls, Dillon Wong, Ryan L. Lee, Xiaomeng Liu, Kenji Watanabe, Takashi Taniguchi, and Ali Yazdani. Evidence for unconventional superconductivity in twisted bilayer graphene. *Nature*, 600(7888):240–245, December 2021.
- [14] Youngjoon Choi, Hyunjin Kim, Cyprian Lewandowski, Yang Peng, Alex Thomson, Robert Polski, Yiran Zhang, Kenji Watanabe, Takashi Taniguchi, Jason Alicea, and Stevan Nadj-Perge. Interaction-driven band flattening and correlated phases in twisted bilayer graphene. *Nat. Phys.*, 17:1375–1381, 2021.
- [15] Jiachen Yu, Benjamin A. Foutty, Zhaoyu Han, Mark E. Barber, Yoni Schattner, Kenji Watanabe, Takashi Taniguchi, Philip Phillips, Zhi-Xun Shen, Steven A. Kivelson, and Benjamin E. Feldman. Correlated Hofstadter spectrum and flavour phase diagram in magic-angle twisted bilayer graphene. *Nature Physics*, April 2022.
- [16] Shaowen Chen, Minhao He, Ya-Hui Zhang, Valerie Hsieh, Zaiyao Fei, K. Watanabe, T. Taniguchi, David H. Cobden, Xiaodong Xu, Cory R. Dean, and Matthew Yankowitz. Electrically tunable correlated and topological states in twisted monolayer–bilayer graphene. *Nature Physics*, 17(3):374–380, oct 2020.
- [17] H. Polshyn, J. Zhu, M. A. Kumar, Y. Zhang, F. Yang, C. L. Tschirhart, M. Serlin, K. Watanabe, T. Taniguchi, A. H. MacDonald, and A. F. Young. Electrical switching of magnetic order in an orbital chern insulator. *Nature*, 588(7836):66–70, nov 2020.
- [18] H. Polshyn, Y. Zhang, M. A. Kumar, T. Soejima, P. Ledwith, K. Watanabe, T. Taniguchi, A. Vishwanath, M. P. Zaletel, and A. F. Young. Topological charge density waves at half-integer filling of a moiré superlattice. *Nature Physics*, 18(1):42–47, dec 2021.
- [19] Canxun Zhang, Tiancong Zhu, Tomohiro Soejima, Salman Kahn, Kenji Watanabe, Takashi Taniguchi, Alex Zettl, Feng Wang, Michael P. Zaletel, and Michael F. Crommie. Local spectroscopy of a gate-switchable moiré quantum anomalous hall insulator. *Nature Communications*, 14(1), jun 2023.
- [20] Yuan Cao, Daniel Rodan-Legrain, Oriol Rubies-Bigorda, Jeong Min Park, Kenji Watanabe, Takashi Taniguchi, and Pablo Jarillo-Herrero. Tunable correlated states and spin-polarized phases in twisted bilayer–bilayer graphene. *Nature*, 583(7815):215–220, may 2020.
- [21] G. William Burg, Jihang Zhu, Takashi Taniguchi, Kenji Watanabe, Allan H. MacDonald, and Emanuel Tutuc. Correlated insulating states in twisted double bilayer graphene. *Physical Review Letters*, 123(19), nov 2019.
- [22] Xiaomeng Liu, Zeyu Hao, Eslam Khalaf, Jong Yeon Lee, Yuval Ronen, Hyobin Yoo, Danial Haei Najafabadi, Kenji Watanabe, Takashi Taniguchi, Ashvin Vishwanath, and Philip Kim. Tunable spin-polarized correlated states in twisted double bilayer graphene. *Nature*, 583(7815):221–225, jul 2020.
- [23] Minhao He, Yuhao Li, Jiaqi Cai, Yang Liu, K Watanabe, Takashi Taniguchi, Xiaodong Xu, and Matthew Yankowitz. Symmetry breaking in twisted double bilayer graphene. *Nature Physics*, 17(1):26–30, 2021.
- [24] Cheng Shen, Yanbang Chu, QuanSheng Wu, Na Li, Shuopei Wang, Yanchong Zhao, Jian Tang, Jieying Liu,

- Jinpeng Tian, Kenji Watanabe, et al. Correlated states in twisted double bilayer graphene. *Nature Physics*, 16(5):520–525, 2020.
- [25] Zeyu Hao, A. M. Zimmerman, Patrick Ledwith, Es-lam Khalaf, Danial Haie Najafabadi, Kenji Watanabe, Takashi Taniguchi, Ashvin Vishwanath, and Philip Kim. Electric field-tunable superconductivity in alternating-twist magic-angle trilayer graphene. *Science*, 371(6534):1133–1138, mar 2021.
- [26] Jeong Min Park, Yuan Cao, Kenji Watanabe, Takashi Taniguchi, and Pablo Jarillo-Herrero. Tunable strongly coupled superconductivity in magic-angle twisted trilayer graphene. *Nature*, 590(7845):249–255, feb 2021.
- [27] Jeong Min Park, Yuan Cao, Li-Qiao Xia, Shuwen Sun, Kenji Watanabe, Takashi Taniguchi, and Pablo Jarillo-Herrero. Robust superconductivity in magic-angle multilayer graphene family. *Nature Materials*, 21(8):877–883, jul 2022.
- [28] Li-Qiao Xia, Sergio C. de la Barrera, Aviram Uri, Aaron Sharpe, Yves H. Kwan, Ziyang Zhu, Kenji Watanabe, Takashi Taniguchi, David Goldhaber-Gordon, Liang Fu, Trithap Devakul, and Pablo Jarillo-Herrero. Helical trilayer graphene: a moiré platform for strongly-interacting topological bands, 2023.
- [29] Aviram Uri, Sergio C. de la Barrera, Mallika T. Randeria, Daniel Rodan-Legrain, Trithap Devakul, Philip J. D. Crowley, Nisarga Paul, Kenji Watanabe, Takashi Taniguchi, Ron Lifshitz, Liang Fu, Raymond C. Ashoori, and Pablo Jarillo-Herrero. Superconductivity and strong interactions in a tunable moiré quasicrystal. *Nature*, 620(7975):762–767, jul 2023.
- [30] Haoxin Zhou, Tian Xie, Takashi Taniguchi, Kenji Watanabe, and Andrea F Young. Superconductivity in rhombohedral trilayer graphene. *Nature*, 598(7881):434–438, 2021.
- [31] Tingxin Li, Shengwei Jiang, Bowen Shen, Yang Zhang, Lizhong Li, Zui Tao, Trithap Devakul, Kenji Watanabe, Takashi Taniguchi, Liang Fu, Jie Shan, and Kin Fai Mak. Quantum anomalous hall effect from intertwined moiré bands. *Nature*, 600(7890):641–646, dec 2021.
- [32] Wenjin Zhao, Kaifei Kang, Lizhong Li, Charles Tschirhart, Evgeny Redekop, Kenji Watanabe, Takashi Taniguchi, Andrea Young, Jie Shan, and Kin Fai Mak. Realization of the haldane chern insulator in a moiré lattice, 2022.
- [33] Benjamin A. Foutty, Carlos R. Kometter, Trithap Devakul, Aidan P. Reddy, Kenji Watanabe, Takashi Taniguchi, Liang Fu, and Benjamin E. Feldman. Mapping twist-tuned multi-band topology in bilayer wse₂, 2023.
- [34] Jiaqi Cai, Eric Anderson, Chong Wang, Xiaowei Zhang, Xiaoyu Liu, William Holtzmann, Yinong Zhang, Fengren Fan, Takashi Taniguchi, Kenji Watanabe, et al. Signatures of fractional quantum anomalous hall states in twisted mote2. *Nature*, pages 1–3, 2023.
- [35] Yihang Zeng, Zhengchao Xia, Kaifei Kang, Jiacheng Zhu, Patrick Knüppel, Chirag Vaswani, Kenji Watanabe, Takashi Taniguchi, Kin Fai Mak, and Jie Shan. Thermodynamic evidence of fractional chern insulator in moiré mote2. *Nature*, pages 1–2, 2023.
- [36] Heonjoon Park, Jiaqi Cai, Eric Anderson, Yinong Zhang, Jiayi Zhu, Xiaoyu Liu, Chong Wang, William Holtzmann, Chaowei Hu, Zhaoyu Liu, et al. Observation of fractionally quantized anomalous hall effect. *Nature*, pages 1–3, 2023.
- [37] Fan Xu, Zheng Sun, Tongtong Jia, Chang Liu, Cheng Xu, Chushan Li, Yu Gu, Kenji Watanabe, Takashi Taniguchi, Bingbing Tong, et al. Observation of integer and fractional quantum anomalous hall effects in twisted bilayer mote 2. *Physical Review X*, 13(3):031037, 2023.
- [38] Eric Anderson, Feng-Ren Fan, Jiaqi Cai, William Holtzmann, Takashi Taniguchi, Kenji Watanabe, Di Xiao, Wang Yao, and Xiaodong Xu. Programming correlated magnetic states with gate-controlled moiré geometry. *Science*, page eadg4268, 2023.
- [39] Anna M. Seiler, Fabian R. Geisenhof, Felix Winterer, Kenji Watanabe, Takashi Taniguchi, Tianyi Xu, Fan Zhang, and R. Thomas Weitz. Quantum cascade of correlated phases in trigonally warped bilayer graphene. *Nature*, 608(7922):298–302, August 2022.
- [40] Guorui Chen, Aaron L. Sharpe, Eli J. Fox, Ya-Hui Zhang, Shaoxin Wang, Lili Jiang, Bosai Lyu, Hongyuan Li, Kenji Watanabe, Takashi Taniguchi, Zhiwen Shi, T. Senthil, David Goldhaber-Gordon, Yuanbo Zhang, and Feng Wang. Tunable correlated chern insulator and ferromagnetism in a moirésuperlattice. *Nature*, 579(7797):56–61, 2020.
- [41] Haoxin Zhou, Tian Xie, Areg Ghazaryan, Tobias Holder, James R Ehrets, Eric M Spanton, Takashi Taniguchi, Kenji Watanabe, Erez Berg, Maksym Serbyn, et al. Half-and quarter-metals in rhombohedral trilayer graphene. *Nature*, 598(7881):429–433, 2021.
- [42] Zhengguang Lu, Tonghang Han, Yuxuan Yao, Aidan P Reddy, Jixiang Yang, Junseok Seo, Kenji Watanabe, Takashi Taniguchi, Liang Fu, and Long Ju. Fractional quantum anomalous hall effect in a graphene moire superlattice. *arXiv preprint arXiv:2309.17436*, 2023.
- [43] Tonghang Han, Zhengguang Lu, Giovanni Scuri, Jiho Sung, Jue Wang, Tianyi Han, Kenji Watanabe, Takashi Taniguchi, Hongkun Park, and Long Ju. Correlated insulator and chern insulators in pentalayer rhombohedral-stacked graphene. *Nature Nanotechnology*, oct 2023.
- [44] Tonghang Han, Zhengguang Lu, Yuxuan Yao, Jixiang Yang, Junseok Seo, Chiho Yoon, Kenji Watanabe, Takashi Taniguchi, Liang Fu, Fan Zhang, and Long Ju. Large quantum anomalous hall effect in spin-orbit proximitized rhombohedral graphene, 2023.
- [45] Guorui Chen, Aaron L. Sharpe, Eli J. Fox, Shaoxin Wang, Bosai Lyu, Lili Jiang, Hongyuan Li, Kenji Watanabe, Takashi Taniguchi, Michael F. Crommie, Marc A. Kastner, Zhiwen Shi, David Goldhaber-Gordon, Yuanbo Zhang, and Feng Wang. Tunable orbital ferromagnetism at noninteger filling of a moiré superlattice. *Nano Letters*, 22(1):238–245, 2022. PMID: 34978444.
- [46] Eric M. Spanton, Alexander A. Zibrov, Haoxin Zhou, Takashi Taniguchi, Kenji Watanabe, Michael P. Zaletel, and Andrea F. Young. Observation of fractional chern insulators in a van der waals heterostructure. *Science*, 360(6384):62–66, apr 2018.
- [47] Haoxin Zhou, Ludwig Holleis, Yu Saito, Liam Cohen, William Huynh, Caitlin L. Patterson, Fangyuan Yang, Takashi Taniguchi, Kenji Watanabe, and Andrea F. Young. Isospin magnetism and spin-polarized superconductivity in bernal bilayer graphene. *Science*, 375(6582):774–778, 2022.

- [48] Yiran Zhang, Robert Polski, Alex Thomson, Étienne Lantagne-Hurtubise, Cyprian Lewandowski, Haoxin Zhou, Kenji Watanabe, Takashi Taniguchi, Jason Alicea, and Stevan Nadj-Perge. Enhanced superconductivity in spin-orbit proximitized bilayer graphene. *Nature*, 613(7943):268–273, Jan 2023.
- [49] Ludwig Holleis, Caitlin L. Patterson, Yiran Zhang, Heun Mo Yoo, Haoxin Zhou, Takashi Taniguchi, Kenji Watanabe, Stevan Nadj-Perge, and Andrea F. Young. Ising superconductivity and nematicity in bernal bilayer graphene with strong spin orbit coupling, 2023.
- [50] Guorui Chen, Aaron L. Sharpe, Patrick Gallagher, Ilan T. Rosen, Eli J. Fox, Lili Jiang, Bosai Lyu, Hongyuan Li, Kenji Watanabe, Takashi Taniguchi, Jeil Jung, Zhiwen Shi, David Goldhaber-Gordon, Yuanbo Zhang, and Feng Wang. Signatures of tunable superconductivity in a trilayer graphene moiré superlattice. *Nature*, 572(7768):215–219, Aug 2019.
- [51] Yongjin Lee, Shi Che, Jairo Velasco Jr., Xueshi Gao, Yanmeng Shi, David Tran, Jacopo Baima, Francesco Mauri, Matteo Calandra, Marc Bockrath, and Chun Ning Lau. Gate-tunable magnetism and giant magnetoresistance in suspended rhombohedral-stacked few-layer graphene. *Nano Letters*, 22(13):5094–5099, Jul 2022.
- [52] Alexander Kerelsky, Carmen Rubio-Verdú, Lede Xian, Dante M. Kennes, Dorri Halbertal, Nathan Finney, Larry Song, Simon Turkel, Lei Wang, Kenji Watanabe, and et al. Moiréless correlations in abca graphene. *Proceedings of the National Academy of Sciences*, 118(4), 2021.
- [53] Kai Liu, Jian Zheng, Yating Sha, Bosai Lyu, Fengping Li, Youngju Park, Yulu Ren, Kenji Watanabe, Takashi Taniguchi, Jinfeng Jia, Weidong Luo, Zhiwen Shi, Jeil Jung, and Guorui Chen. Interaction-driven spontaneous broken-symmetry insulator and metals in abca tetralayer graphene, 2023.
- [54] Tonghang Han, Zhenguang Lu, Giovanni Scuri, Jiho Sung, Jue Wang, Tianyi Han, Kenji Watanabe, Takashi Taniguchi, Liang Fu, Hongkun Park, and Long Ju. Orbital multiferroicity in pentalayer rhombohedral graphene. *Nature*, 623(7985):41–47, Nov 2023.
- [55] Yating Sha, Jian Zheng, Kai Liu, Hong Du, Kenji Watanabe, Takashi Taniguchi, Jinfeng Jia, Zhiwen Shi, Ruidan Zhong, and Guorui Chen. Observation of chern insulator in crystalline abca-tetralayer graphene with spin-orbit coupling. *arXiv preprint arXiv:2310.17971*, 2023.
- [56] Ya-Hui Zhang, Dan Mao, Yuan Cao, Pablo Jarillo-Herrero, and T. Senthil. Nearly flat chern bands in moiré superlattices. *Phys. Rev. B*, 99:075127, Feb 2019.
- [57] Bheema Lingam Chittari, Guorui Chen, Yuanbo Zhang, Feng Wang, and Jeil Jung. Gate-tunable topological flat bands in trilayer graphene boron-nitride moiré superlattices. *Phys. Rev. Lett.*, 122:016401, Jan 2019.
- [58] Cécile Repellin, Zhihuan Dong, Ya-Hui Zhang, and T. Senthil. Ferromagnetism in narrow bands of moiré superlattices. *Phys. Rev. Lett.*, 124:187601, May 2020.
- [59] Ya-Hui Zhang and T. Senthil. Bridging hubbard model physics and quantum hall physics in trilayer graphene/h – BN moiré superlattice. *Phys. Rev. B*, 99:205150, May 2019.
- [60] Matthew Yankowitz, Shaowen Chen, Hryhorii Polshyn, Yuxuan Zhang, K. Watanabe, T. Taniguchi, David Graf, Andrea F. Young, and Cory R. Dean. Tuning superconductivity in twisted bilayer graphene. *Science*, 363(6431):1059–1064, 2019.
- [61] Yonglong Xie, Andrew T. Pierce, Jeong Min Park, Daniel E. Parker, Eslam Khalaf, Patrick Ledwith, Yuan Cao, Seung Hwan Lee, Shaowen Chen, Patrick R. Forrester, Kenji Watanabe, Takashi Taniguchi, Ashvin Vishwanath, Pablo Jarillo-Herrero, and Amir Yacoby. Fractional Chern insulators in magic-angle twisted bilayer graphene. *Nature*, 600(7889):439–443, December 2021.
- [62] Pilkyung Moon and Mikito Koshino. Electronic properties of graphene/hexagonal-boron-nitride moiré superlattice. *Physical Review B*, 90(15):155406, 2014.
- [63] Jeil Jung, Arnaud Raoux, Zhenhua Qiao, and A. H. MacDonald. Ab initio theory of moiré superlattice bands in layered two-dimensional materials. *Phys. Rev. B*, 89:205414, May 2014.
- [64] Jeil Jung, Evan Laksono, Ashley M DaSilva, Allan H MacDonald, Marcin Mucha-Kruczyński, and Shaffique Adam. Moiré band model and band gaps of graphene on hexagonal boron nitride. *Physical Review B*, 96(8):085442, 2017.
- [65] Lukas PA Krisna and Mikito Koshino. Moiré phonons in graphene/hexagonal boron nitride moiré superlattice. *Physical Review B*, 107(11):115301, 2023.
- [66] Adarsh S. Patri and T. Senthil. Strong correlations in abc-stacked trilayer graphene: Moiré is important. *Phys. Rev. B*, 107:165122, Apr 2023.
- [67] Cécile Repellin, Zhihuan Dong, Ya-Hui Zhang, and T. Senthil. Ferromagnetism in narrow bands of moiré superlattices. *Phys. Rev. Lett.*, 124:187601, May 2020.
- [68] Yonglong Xie, Andrew T. Pierce, Jeong Min Park, Daniel E. Parker, Eslam Khalaf, Patrick Ledwith, Yuan Cao, Seung Hwan Lee, Shaowen Chen, Patrick R. Forrester, Kenji Watanabe, Takashi Taniguchi, Ashvin Vishwanath, Pablo Jarillo-Herrero, and Amir Yacoby. Fractional chern insulators in magic-angle twisted bilayer graphene. *Nature*, 600(7889):439–443, 2021.
- [69] Daniel Parker, Patrick Ledwith, Eslam Khalaf, Tomohiro Soejima, Johannes Hauschild, Yonglong Xie, Andrew Pierce, Michael P Zaletel, Amir Yacoby, and Ashvin Vishwanath. Field-tuned and zero-field fractional chern insulators in magic angle graphene. *arXiv preprint arXiv:2112.13837*, 2021.
- [70] Patrick J. Ledwith, Grigory Tarnopolsky, Eslam Khalaf, and Ashvin Vishwanath. Fractional chern insulator states in twisted bilayer graphene: An analytical approach. *Phys. Rev. Research*, 2:023237, May 2020.
- [71] Ahmed Abouelkomsan, Kang Yang, and Emil J. Bergholtz. Quantum metric induced phases in moiré materials. *Phys. Rev. Res.*, 5:L012015, Feb 2023.
- [72] Cécile Repellin and T. Senthil. Chern bands of twisted bilayer graphene: Fractional chern insulators and spin phase transition. *Phys. Rev. Research*, 2:023238, May 2020.
- [73] Nick Bultinck, Shubhayu Chatterjee, and Michael P. Zaletel. Mechanism for anomalous hall ferromagnetism in twisted bilayer graphene. *Phys. Rev. Lett.*, 124:166601, Apr 2020.
- [74] Ming Xie and A. H. MacDonald. Nature of the correlated insulator states in twisted bilayer graphene. *Phys. Rev. Lett.*, 124:097601, Mar 2020.
- [75] Liujun Zou, Hoi Chun Po, Ashvin Vishwanath, and

- T. Senthil. Band structure of twisted bilayer graphene: Emergent symmetries, commensurate approximants, and wigner obstructions. *Phys. Rev. B*, 98:085435, Aug 2018.
- [76] Ya-Hui Zhang, Dan Mao, and T. Senthil. Twisted bilayer graphene aligned with hexagonal boron nitride: Anomalous hall effect and a lattice model. *Phys. Rev. Res.*, 1:033126, Nov 2019.
- [77] Fengcheng Wu, Timothy Lovorn, Emanuel Tutuc, Ivar Martin, and AH MacDonald. Topological insulators in twisted transition metal dichalcogenide homobilayers. *Physical review letters*, 122(8):086402, 2019.
- [78] B. I. Halperin, Z. Tesanović, and F. Axel. Compatibility of crystalline order and the quantized hall effect. *Phys. Rev. Lett.*, 57:922–922, Aug 1986.
- [79] Zlatko Tesanović, Françoise Axel, and B. I. Halperin. “hall crystal” versus wigner crystal. *Phys. Rev. B*, 39:8525–8551, Apr 1989.
- [80] Fan Zhang, Bhagawan Sahu, Hongki Min, and Allan H MacDonald. Band structure of a b c-stacked graphene trilayers. *Physical Review B*, 82(3):035409, 2010.
- [81] Jeil Jung and Allan H MacDonald. Gapped broken symmetry states in abc-stacked trilayer graphene. *Physical Review B*, 88(7):075408, 2013.
- [82] We estimate the conversion between D and u_D by comparing the reported HF phase diagram with the experiment in rhombohedral trilayer graphene [41, 107].
- [83] Youngju Park, Yeonju Kim, Bheema Lingam Chittari, and Jeil Jung. Topological flat bands in rhombohedral tetralayer and multilayer graphene on hexagonal boron nitride moire superlattices, 2023.
- [84] N. Regnault and B. Andrei Bernevig. Fractional chern insulator. *Phys. Rev. X*, 1:021014, Dec 2011.
- [85] D. N. Sheng, Zheng-Cheng Gu, Kai Sun, and L. Sheng. Fractional quantum hall effect in the absence of landau levels. *Nature Communications*, 2(1):389, 2011.
- [86] Titus Neupert, Luiz Santos, Claudio Chamon, and Christopher Mudry. Fractional quantum hall states at zero magnetic field. *Phys. Rev. Lett.*, 106:236804, Jun 2011.
- [87] Hui Li and F. D. M. Haldane. Entanglement spectrum as a generalization of entanglement entropy: Identification of topological order in non-abelian fractional quantum hall effect states. *Phys. Rev. Lett.*, 101:010504, Jul 2008.
- [88] Rahul Roy. Band geometry of fractional topological insulators. *Phys. Rev. B*, 90:165139, Oct 2014.
- [89] Siddharth A. Parameswaran, Rahul Roy, and Shivaji L. Sondhi. Fractional quantum hall physics in topological flat bands. *Comptes Rendus Physique*, 14(9-10):816–839, nov 2013.
- [90] T. S. Jackson, Gunnar Möller, and Rahul Roy. Geometric stability of topological lattice phases. *Nature Communications*, 6(1):8629, 2015.
- [91] Martin Claassen, Ching Hua Lee, Ronny Thomale, Xiao-Liang Qi, and Thomas P. Devereaux. Position-momentum duality and fractional quantum hall effect in chern insulators. *Phys. Rev. Lett.*, 114:236802, Jun 2015.
- [92] Grigory Tarnopolsky, Alex Jura Kruchkov, and Ashvin Vishwanath. Origin of magic angles in twisted bilayer graphene. *Phys. Rev. Lett.*, 122:106405, Mar 2019.
- [93] Tomoki Ozawa and Bruno Mera. Relations between topology and the quantum metric for chern insulators. *Phys. Rev. B*, 104:045103, Jul 2021.
- [94] Bruno Mera and Tomoki Ozawa. Kähler geometry and chern insulators: Relations between topology and the quantum metric. *Phys. Rev. B*, 104:045104, Jul 2021.
- [95] Bruno Mera and Tomoki Ozawa. Engineering geometrically flat chern bands with fubini-study kähler structure. *Phys. Rev. B*, 104:115160, Sep 2021.
- [96] Jie Wang, Jennifer Cano, Andrew J. Millis, Zhao Liu, and Bo Yang. Exact landau level description of geometry and interaction in a flatband. *Phys. Rev. Lett.*, 127:246403, Dec 2021.
- [97] Jie Wang and Zhao Liu. Hierarchy of ideal flatbands in chiral twisted multilayer graphene models. *Phys. Rev. Lett.*, 128:176403, Apr 2022.
- [98] Patrick J. Ledwith, Ashvin Vishwanath, and Daniel E. Parker. Vortexability: A Unifying Criterion for Ideal Fractional Chern Insulators. *arXiv e-prints*, page arXiv:2209.15023, September 2022.
- [99] Jie Wang, Semyon Klevtsov, and Zhao Liu. Origin of model fractional chern insulators in all topological ideal flatbands: Explicit color-entangled wave function and exact density algebra. *Phys. Rev. Res.*, 5:023167, Jun 2023.
- [100] Junkai Dong, Patrick J. Ledwith, Eslam Khalaf, Jong Yeon Lee, and Ashvin Vishwanath. Many-body ground states from decomposition of ideal higher chern bands: Applications to chirally twisted graphene multilayers. *Phys. Rev. Res.*, 5:023166, Jun 2023.
- [101] Kai Sun, Zhengcheng Gu, Hoshio Katsura, and S. Das Sarma. Nearly flatbands with nontrivial topology. *Phys. Rev. Lett.*, 106:236803, Jun 2011.
- [102] Yi-Fei Wang, Zheng-Cheng Gu, Chang-De Gong, and D. N. Sheng. Fractional quantum hall effect of hard-core bosons in topological flat bands. *Phys. Rev. Lett.*, 107:146803, Sep 2011.
- [103] Evelyn Tang, Jia-Wei Mei, and Xiao-Gang Wen. High-temperature fractional quantum hall states. *Phys. Rev. Lett.*, 106:236802, Jun 2011.
- [104] J. R. Trail, M. D. Towler, and R. J. Needs. Unrestricted hartree-fock theory of wigner crystals. *Physical Review B*, 68(4), jul 2003.
- [105] Zhihuan Dong, Adarsh S. Patri, and T. Senthil. Theory of fractional quantum anomalous hall phases in pentilayer rhombohedral graphene moiré structures, 2023.
- [106] Boran Zhou, Hui Yang, and Ya-Hui Zhang. Fractional quantum anomalous hall effects in rhombohedral multilayer graphene in the moiréless limit and in coulomb imprinted superlattice, 2023.
- [107] Shubhayu Chatterjee, Taige Wang, Erez Berg, and Michael P Zaletel. Inter-valley coherent order and isospin fluctuation mediated superconductivity in rhombohedral trilayer graphene. *Nature communications*, 13(1):6013, 2022.
- [108] Guorui Chen, Aaron L Sharpe, Patrick Gallagher, Ilan T Rosen, Eli J Fox, Lili Jiang, Bosai Lyu, Hongyuan Li, Kenji Watanabe, Takashi Taniguchi, et al. Signatures of tunable superconductivity in a trilayer graphene moiré superlattice. *Nature*, 572(7768):215–219, 2019.
- [109] Areg Ghazaryan, Tobias Holder, Erez Berg, and Maksym Serbyn. Multilayer graphenes as a platform for interaction-driven physics and topological superconductivity. *Physical Review B*, 107(10):104502, 2023.
- [110] Taige Wang, Marc Vila, Michael P Zaletel, and Shub-

Aside from lattice translation, the model enjoys the following symmetries

$$\overline{h(\mathbf{k})} = h(-\mathbf{k}) \quad (\text{Time reversal}) \quad (\text{A7a})$$

$$h(\mathbf{k}) = h(C_{3z}\mathbf{k}) \quad (\text{Three fold rotation}) \quad (\text{A7b})$$

$$M_{C_{2x}}h(\mathbf{k})M_{C_{2x}}^{-1} = h(C_{2x}\mathbf{k}) \quad (\text{Two-fold } x\text{-rotation}) \quad (\text{A7c})$$

$$h(\mathbf{k}) = h(M_x\mathbf{k}) \quad (\text{Mirror}) \quad (\text{A7d})$$

$$V_{\mathbf{G}}h(\mathbf{k})V_{\mathbf{G}}^\dagger = h(\mathbf{k} + \mathbf{G}) \quad (\mathbf{G}\text{-translation}) \quad (\text{A7e})$$

where time-reversal acts anti-unitarily, C_{2x} reverses layers as $[M_{C_{2x}}]_{\sigma\ell,\sigma'\ell'} = \delta_{\sigma,-\sigma'}\delta_{\ell,N-(\ell'+1)}$, and other symmetries have trivial orbital part. We note that the last equation is not a symmetry per se, but simply a constraint on the Hamiltonian with $[V_{\mathbf{G}}]_{\sigma'\ell',\sigma\ell} = \delta_{\sigma\sigma'}\delta_{\ell\ell'}e^{i\mathbf{G}\cdot\mathbf{r}_{\sigma,\ell}}$, reflecting the unit cell embedding.

2. Moiré Rhombohedral Graphene Hamiltonian

The direct lattice of the hBN substrate is generated by

$$\mathbf{R}'_j = MR_\theta\mathbf{R}_j; \quad M = (1 + \varepsilon)I \quad (\text{A8})$$

where R_θ is counterclockwise rotation by θ and $\varepsilon = a_{\text{hBN}}/a_{\text{Gr}} \approx 1.018$. We take \mathbf{G}'_j such that $\mathbf{R}'_j \cdot \mathbf{G}'_k = 2\pi\delta_{jk}$ as usual.

Define moiré reciprocal lattice vectors

$$\mathbf{g}_j = \mathbf{G}_j - \mathbf{G}'_j = [I - M^{-1}R_\theta]\mathbf{G}_j, \quad (\text{A9})$$

with corresponding direct vectors $\mathbf{a}_j \cdot \mathbf{g}_k = 2\pi\delta_{jk}$ whose moiré superlattice period is

$$L_M = |\mathbf{a}_j| = a \frac{1 + \varepsilon}{\sqrt{\varepsilon^2 + 2(1 + \varepsilon)(1 - \cos\theta)}} \quad (\text{A10})$$

and where the lattice scale mismatch rotates the moiré Brillouin zone so that \mathbf{a}_1 is rotated clockwise from the x axis by an angle

$$\phi = \arctan\left(\frac{-\sin\theta}{1 + \varepsilon - \cos\theta}\right). \quad (\text{A11})$$

As θ changes from 0 to 1, the superlattice scale changes only gradually, but ϕ rotates quickly, as shown in Fig. 5.

To conveniently express C_3 -symmetric quantities, further define $\mathbf{g}_3 = -\mathbf{g}_1 - \mathbf{g}_2$ and likewise for $\mathbf{G}_3, \mathbf{G}'_3$. We then have high-symmetry points at

$$\begin{aligned} \gamma &= \mathbf{K}_{\text{Gr}}, \quad \kappa^+ = \gamma - \frac{1}{3}\mathbf{g}_1 + \frac{1}{3}\mathbf{g}_2, \\ \kappa^- &= \gamma - \frac{2}{3}\mathbf{g}_1 - \frac{1}{3}\mathbf{g}_2, \quad \mu = \gamma - \frac{1}{2}\mathbf{g}_1. \end{aligned} \quad (\text{A12})$$

Crucially, we have taken the center of the moiré Brillouin zone γ to be at the \mathbf{K} -point of graphene.

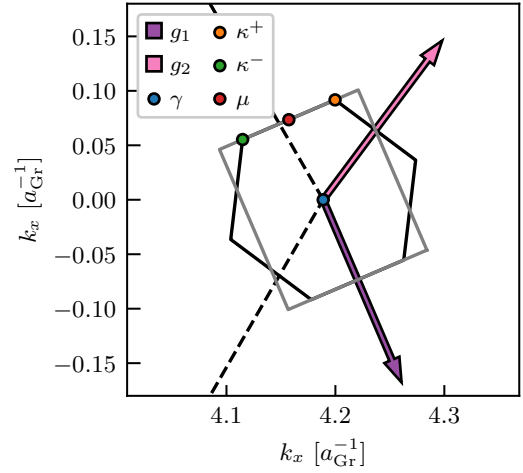


FIG. 5. Geometry of the moiré Brillouin zone at $\theta = 0.77^\circ$. The dashed line is the Brillouin zone of (unrotated) graphene, and the gray rectangle is the Brillouin zone used for DMRG (see text).

We may now express the moiré potential generated by the hBN substrate. We assume that the moiré potential of the hBN substrate only affects the closest layer. We follow [62] (which uses an opposite valley convention), we have

$$V_{\text{hBN}}(\mathbf{r}) = V_0\sigma^0 + V_1\mathbf{f}(\mathbf{r}, \psi) \cdot \boldsymbol{\sigma}, \quad (\text{A13})$$

where

$$\begin{aligned} \mathbf{f}(\mathbf{r}, \psi) \cdot \boldsymbol{\sigma} &= e^{-i\psi} \left[e^{i\mathbf{g}_1 \cdot \mathbf{r}} \begin{pmatrix} 1 & 1 \\ \omega & \omega \end{pmatrix} + e^{i\mathbf{g}_2 \cdot \mathbf{r}} \begin{pmatrix} 1 & \omega^2 \\ \omega^2 & \omega \end{pmatrix} \right. \\ &\quad \left. + e^{-i(\mathbf{g}_1 + \mathbf{g}_2) \cdot \mathbf{r}} \begin{pmatrix} 1 & \omega \\ 1 & \omega \end{pmatrix} \right] + \text{H.c.} \end{aligned} \quad (\text{A14})$$

Unless otherwise stated we take values $(V_0, V_1, \psi) = (28.9 \text{ meV}, 21 \text{ meV}, -0.29)$ following [62]. The Hamiltonian in the K' valley is defined via time-reversal symmetry.

3. Many-Body Hamiltonian

Let the single-particle eigenstates be given by

$$\hat{h}_{kin} |\psi_{\mathbf{k}\tau sb}\rangle = \epsilon_{\mathbf{k}\tau sb} |\psi_{\mathbf{k}\tau sb}\rangle \quad (\text{A15})$$

where $\tau \in \{K, K'\} = \{-1, 1\}$ labels valley, $s \in \{\uparrow, \downarrow\} = \{-1, 1\}$ labels spin, and b labels bands. Consider creation operators

$$c_{\mathbf{k}\tau sb}^\dagger |0\rangle = |\psi_{\mathbf{k}\tau sb}\rangle, \quad \{c_{\mathbf{k}\tau sb}, c_{\mathbf{k}'\tau's'b'}\} = \delta_{\mathbf{k}\mathbf{k}'} \delta_{\tau\tau'} \delta_{ss'} \delta_{bb'}. \quad (\text{A16})$$

We consider the interacting model

$$\hat{H} = \hat{h}_{kin} + \frac{1}{2A} \sum_{\mathbf{q}} U_{|\mathbf{q}|} : \hat{\rho}_{\mathbf{q}} \hat{\rho}_{-\mathbf{q}} :; U_{\mathbf{q}} = \frac{2\pi \tanh(qd)}{\epsilon_r \epsilon_0 q} \quad (\text{A17})$$

where U_q represents Coulomb interactions screened by both top and bottom gates at a distance of $d = 250 \text{ \AA}$.

To make the Hilbert space tractable, we restrict to a limited number of bands N_b above charge neutrality. (Alternatively one could use a plane-wave basis and use some number of shells of Brillouin zones around the first.) More explicitly, we work with the projected density operator,

$$\hat{\rho}_{\mathbf{q}} = \sum_{\mathbf{k}} \sum_{\alpha, \beta} \sum_{b, b' < N_b} \hat{c}_{\mathbf{k}\alpha b}^\dagger \langle \psi_{\mathbf{k}\alpha b} | e^{-i\mathbf{q}\cdot\mathbf{r}} | \psi_{\mathbf{k}+\mathbf{q}, \beta, b'} \rangle \hat{c}_{\mathbf{k}+\mathbf{q}, \beta, b'} \quad (\text{A18})$$

where α, β index valley, spin, and b, b' labels band. In some contexts such as twisted bilayer graphene, the operation of restricting to low-energy bands is fraught with difficulties due to double-counting of interaction effects, necessitating procedures such as ‘‘Hartree-Fock subtraction’’ [69, 111] or more sophisticated renormalization-group treatments [112]. Happily, here these issues are ameliorated in the limit where the displacement field opens a gap comparable to or larger than the interaction strength. In that case, the insulating state at charge neutrality is a natural choice of vacuum. The operation of integrating out the ‘‘remote’’ higher-energy conduction bands $N_b + 1, N_b + 2, \dots$, and valence bands at mean-field level is equivalent to simply *restricting* the band indices in all sums in Eq. (A17). We note, however, that beyond-mean-field effects like RPA-level screening from remote bands could substantially influence the system. This is often captured at a phenomenological level by increasing the relative dielectric constant ϵ_r .

Appendix B: Details of the Hartree-Fock calculation

We use standard self-consistent Hartree-Fock calculations to obtain the SCHF ground state of the electronic system.

1. Numerical Setup

As usual, we consider single-particle density matrices $P(\mathbf{k})_{\beta\alpha} = \langle c_{\mathbf{k}\beta}^\dagger c_{\mathbf{k}\alpha} \rangle$, where α and β are collective indices for valley, spin, and band. These density matrices are in one-to-one correspondence with Slater determinant states. We define the Hartree and Fock Hamiltonians as

$$h_H[P](\mathbf{k}) = \frac{1}{A} \sum_{\mathbf{g}} V_{\mathbf{g}} \Lambda_{\mathbf{g}}(\mathbf{k}) \left(\sum_{\mathbf{k}} \text{Tr}[P(\mathbf{k}) \Lambda_{\mathbf{g}}(\mathbf{k})^\dagger] \right) \quad (\text{B1a})$$

$$h_F[P](\mathbf{k}) = -\frac{1}{A} \sum_{\mathbf{q}} V_{\mathbf{q}} \Lambda_{\mathbf{q}}(\mathbf{k}) P([\mathbf{k} + \mathbf{q}]) \Lambda_{\mathbf{q}}(\mathbf{k})^\dagger \quad (\text{B1b})$$

where $[\Lambda_{\mathbf{q}}(\mathbf{k})]_{\alpha\beta} = \langle \psi_{\mathbf{k}\alpha} | e^{-i\mathbf{q}\cdot\mathbf{r}} | \psi_{\mathbf{k}+\mathbf{q}\beta} \rangle$ are form factors, and are treated as matrices whose labels are identical to

the single-particle ones. The sum over \mathbf{g} runs over reciprocal vectors while \mathbf{q} runs over all momentum transfers. Via Wick’s theorem, the energy of the Slater-determinant state is

$$E[P] = \frac{1}{2} \text{Tr}[P(2h_{\text{kin}} + h_H[P] + h_F[P])] \quad (\text{B2})$$

where the trace is over momentum and all other band labels.

We use the optimal-damping algorithm (ODA) to converge to states satisfying the self-consistency condition

$$[P, h_{\text{kin}} + h_H[P] + h_F[P]] = 0 \quad (\text{B3})$$

to tolerances approaching the square root of machine precision (i.e. machine precision in $E[P]$). We use both rectangular and Monkhorst-Pack grids with 24×24 , 30×30 , 36×36 , or 48×48 unit cells, depending on the sensitivity of the state to finite-size effects. We impose C_3 symmetry explicitly in the Monkhorst-Pack case, but find comparable results in both cases for sufficiently large system sizes. We ensure that the range of momentum transfers \mathbf{q} considered is sufficiently large to converge the energy of the state, out to several Brillouin zone distances. To avoid non-global minima, we initialize SCHF in a variety of states for each parameter point, often using a mix of physical ansatzes as well as random initial states. Unless otherwise stated, we use $N_b = 7$ bands. The 8th band is fully separated from the lowest filled band for many parameters. Comprehensive SCHF calculations also show vanishing occupation in the 8th band for most HF ground states. We also assume electrons are spin- and valley-polarized.

2. Metal versus Anomalous Hall Crystal Competition

To examine the competition between the metallic ‘‘quarter metal’’ state and the anomalous Hall crystal shown in Fig. 1(b), we must determine the ground state energy both with and without continuous translation symmetry. To do this, we first compute the SCHF ground state of standalone rhombohedral graphene in a patch near the K point that is much bigger than the moiré Brillouin zone, finding a metallic state with enforced continuous translation symmetry. We then compute another SCHF ground state with folded Brillouin zone, which gives the possibility of breaking continuous translation symmetry. No hBN moiré potential is added. At small u_D , the energies from both methods agree to extremely high precision and indeed describe the same quarter-metal state. At a critical u_D , however, the translation-breaking ansatz finds a ground state with an interaction induced gap that is lower energy than the metal — the anomalous Hall crystal described in the main text.

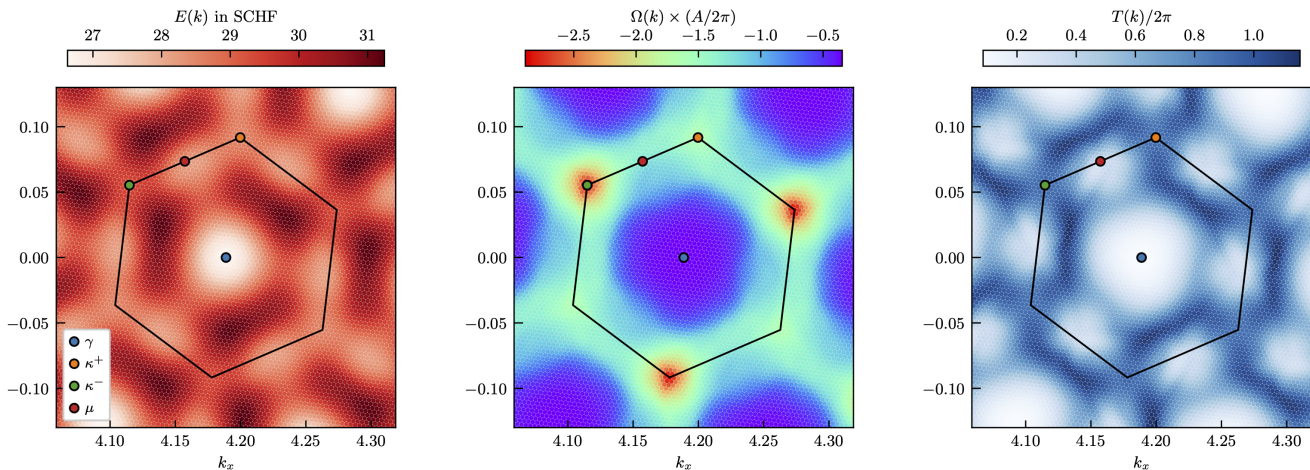


FIG. 6. Details of the SCHF state at $\nu = 1$. (Left) Dispersion. (Middle) Berry curvature. (Right) trace condition violation. Parameters: $\theta = 0.77^\circ$, $D = 50$ meV, 48×48 unit cells.

3. Identification of moiré proximate side from $\nu = 4$ SCHF

To confirm whether our setup of moiré proximate/distant side corresponds to that in experiments, we identify the experiment observation of correlated insulator at $N_L = 5, \nu = 4$ [42]: At low displacement field $|D| < 0.5$ V/nm, corresponding to $u_D \sim 30$ meV, an insulator is found at $D < 0$ side up to $|D| = 0.4$ V/nm, but not at $D > 0$. We now will show that this agrees with our numerical observation at similar u_D , establishing a matching between the two works.

We perform self-consistent Hartree-Fock (SCHF) with both spin and valley degrees of freedom. We only include the conduction band as in the main text, and restrict ourselves to $D \geq 10$ meV where the valence bands are sufficiently separated. At $\nu = 4$, we search for the ground state in the manifold without intervalley coupling, which excludes intervalley coherent (IVC) orders.

We examine the resulting charge gap Δ at different u_D , as shown in Fig. 7, which shows a clear asymmetry between $u_D > 0$ and $u_D < 0$: a charge gap is only identified for $u_D < 0$ but not for $u_D > 0$, which agrees with the experiment described above. This suggests that the experiment identifies $\nu = 4$ insulator only on the moiré proximate regime. Although there could be other competing orders unconsidered here, the identification of the gapless phase is expected to be robust even beyond Hartree-Fock approximations.

4. Details of N_L - u_D phase diagram

Fig.8 shows the extended N_L - u_D phase diagram in Fig.1(a) which we extend up to $u_D = 160$ meV. Each N_L shows similar patterns as $N_L = 5$ discussed in Fig.2(a). First, a broad regime of $C = -1$ AHC phase is stabi-

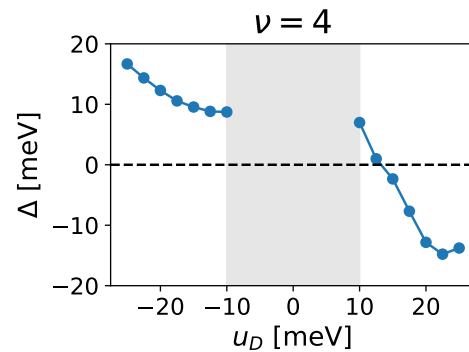


FIG. 7. Charge gap of 30×30 Hartree-Fock ground state at $\nu = 4$ for $N_L = 5, |u_D| = 10 - 25$ meV. Model parameters follow Appendix B 1, but include both spins and valleys.

lized at moderate u_D . The lower critical u_D , referred to as u_D^* in the main text, decreases with N_L , indicating the stronger relevance of AHC in higher- N_L rhombohedral graphenes. Meanwhile, the higher critical u_D is controlled by the development of indirect band gap between $C = -1$ band and higher bands, which leads to a first-order transition into metal (and occasionally the “reentrance” of $C = -1$ state at $N_L = 4$.) At even higher u_D , other phases such as the $C = 0$ insulator take over, but given the stronger band mixing it is necessary to include more bands in SCHF to accurately resolve the phase competition. We therefore caution against trusting the phase diagram at large u_D .

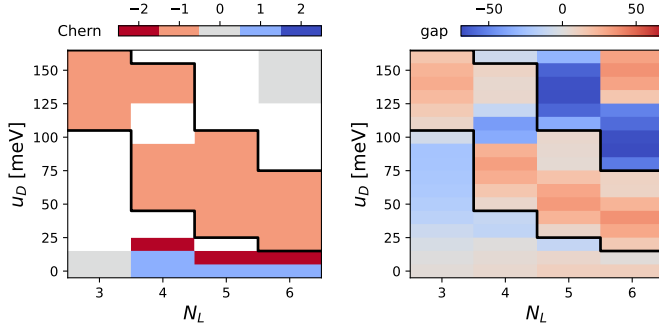


FIG. 8. (a) Chern-number and (b) charge-gap phase diagram at $\nu = 1$ for rhombohedral graphene with $N_L = 3 - 6$ and $u_D = 0 - 160$ meV, with fixed $\theta = 0.77^\circ$ and $\epsilon_r = 5$ at each N_L . Obtained from 36×36 SCHF. The $C = -1$ AHC phase is highlighted with black box. The white region in the Chern-number plot denotes metal with direct or indirect band gap.

Appendix C: Details of the Many-Body Numerics at Fractional Filling

To determine the many-body ground state at fractional filling, we undertake a two-step procedure: (1) solve for the SCHF ground state at filling $\nu = 1$ and then (2) solve the many-body problem restricted to the lowest SCHF band at fractional filling using either exact-diagonalization or the density-matrix renormalization group.

Explicitly, this is done as follows. Consider the SCHF Hamiltonian $h_{HF}[P]$ at $\nu = 1$, which may be diagonalized as

$$h_{HF}[P](\mathbf{k})_{\alpha\beta} U(\mathbf{k})_{\beta\gamma} = U(\mathbf{k})_{\alpha\gamma} E(\mathbf{k})_{\gamma}. \quad (\text{C1})$$

We may then pass to the basis of Hartree-Fock bands

$$|\phi_{\mathbf{k}\alpha}\rangle = |\psi_{\mathbf{k}\beta}\rangle U(\mathbf{k})_{\beta\alpha}, \quad (\text{C2})$$

which constitutes a unitary rotation of our set of N_b low-energy bands. We may then integrate out the $N_b - 1$ bands above the $\nu = 1$ gap at mean-field level — which again is simply an index restriction — to arrive at a one-band Hamiltonian

$$\hat{H} = \sum_{\mathbf{k}} t_{\mathbf{k}} \hat{n}_{\mathbf{k}} + \frac{1}{2A} \sum_{\mathbf{q}, \mathbf{k}, \mathbf{k}'} U_{\mathbf{q}} \lambda_{\mathbf{q}}(\mathbf{k}) \lambda_{-\mathbf{q}}(\mathbf{k}') \hat{d}_{\mathbf{k}}^{\dagger} \hat{d}_{\mathbf{k}'}^{\dagger} \hat{d}_{\mathbf{k}'-\mathbf{q}} \hat{d}_{\mathbf{k}+\mathbf{q}}, \quad (\text{C3})$$

where $\hat{d}_{\mathbf{k}} |0\rangle = |\phi_{\mathbf{k}0}\rangle$ is a creation operator for the lowest SCHF band, a band with form factors $\lambda_{\mathbf{q}}(\mathbf{k}) = \langle \phi_{\mathbf{k}0} | e^{-i\mathbf{q}\cdot\mathbf{r}} | \phi_{\mathbf{k}+\mathbf{q}0} \rangle$, and $\hat{n}_{\mathbf{k}} = \hat{d}_{\mathbf{k}}^{\dagger} \hat{d}_{\mathbf{k}}$.

For exact diagonalization, we solve the SCHF problem on 36×36 \mathbf{k} -points, then restrict Eq. (C3) to size 4×6 . Varying the base point for the subsampling allows for flux

insertion, which demonstrates the spectral flow between the three quasidegenerate FCI ground states.

To apply the density-matrix renormalization group, we follow previous work on moiré DMRG systems [113–116] to place the system onto an infinite cylinder geometry. We start with a rectangular moiré Brillouin zone, shown in Fig. 5, with side lengths $B_1 = |\mathbf{g}_1|$, $B_2 = \frac{\sqrt{3}}{2} |\mathbf{g}_2|$. We impose periodic boundary conditions in the “2” direction corresponding to momentum discretization

$$k_2[n] = B_2 \times \begin{cases} -\frac{1}{2} + \frac{n + \frac{\Phi_2}{2\pi}}{N_2} & \text{if } N_2 \equiv 0 \pmod{2} \\ -\frac{1}{2} + \frac{n + \frac{\Phi_2}{2\pi} + \frac{1}{2}}{N_2} & \text{if } N_2 \equiv 1 \pmod{2} \end{cases}, \quad (\text{C4})$$

relative to an origin at moiré- γ . This gives N_2 evenly spaced “wires” across the Brillouin zone, which intersect the γ point for flux $\Phi_2 = 0$.

We then take a basis of hybrid Wannier functions along each wire, i.e. maximally localized along \mathbf{a}_1 and periodic along \mathbf{a}_2 :

$$|w_{n,k_2}\rangle = \frac{1}{\sqrt{N_1}} \sum_{\mathbf{k}_1} |\varphi_{\mathbf{k}}\rangle e^{-i\mathbf{n}\mathbf{k}\cdot\mathbf{a}_1}; \quad |\varphi_{\mathbf{k}}\rangle = |\phi_{\mathbf{k}0}\rangle e^{i\zeta(\mathbf{k})}. \quad (\text{C5})$$

Here the gauge choice $\zeta(\mathbf{k})$ is chosen such that

$$\hat{T}_1 |w^{n,k_2}\rangle = |w^{n-1,k_2}\rangle \quad (\text{C6a})$$

$$\hat{T}_2 |w^{n,k_2}\rangle = e^{i2\pi k_2/B_2} |w^{n,k_2}\rangle \quad (\text{C6b})$$

$$\hat{P} e^{-i\hat{r}_1 B_1} \hat{P} |w^{n,k_2}\rangle = e^{i2\pi P_1(k_2)} |w^{n,k_2}\rangle \quad (\text{C6c})$$

where the polarizations $P_1(k_2) = \frac{B_1}{2\pi} \langle w^{0,k_2} | \hat{r}_1 | w^{0,k_2} \rangle$ are the centers of the Wannier orbitals in the first unit cell, in accordance with the modern theory of polarization [117]. The Hamiltonian (C3) can be straightforwardly expressed in terms of fermion operators $f_{n,k_2}^{\dagger} |0\rangle = |w_{n,k_2}\rangle$ on an infinite cylinder geometry. As this is a long-ranged, two-dimensional Hamiltonian, working with it efficiently as a matrix product operator (MPO) requires the technique of “MPO Compression” developed by some of us [113, 118], which creates a faithful low-rank approximation of the Hamiltonian with errors below the 10^{-2} meV level.

We then apply standard DMRG using the open-source tenpy [119] library. We work at cylinder circumference $L_y = 8$. We converge the ground state to norm error below 10^{-13} on bond dimensions up to $\chi = 1536$ — since the state is fully-gapped, only moderate bond dimensions are required. To diagnose the fractional Chern insulator we use the entanglement spectrum technique first proposed by [87], finding the characteristic degeneracy counting matching partition numbers 1, 1, 2, 3, 5, 7, ... for each bond. We have also verified this holds for $L_y = 5, 6$.